Pressure Dependence of the Glass Transition in Atactic and Isotactic Polypropylene

A. Gitsas and G. Floudas*

Department of Physics, University of Ioannina, Post Office Box 1186, GR-45110 Ioannina, Greece, and Foundation for Research and Technology-Hellas (FORTH), Biomedical Research Institute (BRI), GR-71110 Heraklion, Crete, Greece

Received July 6, 2008; Revised Manuscript Received October 21, 2008

ABSTRACT: The segmental relaxation process in atactic and isotactic polypropylene (PP) is studied over the temperature (258−323 K) and pressure (0−300 MPa) ranges by means of dielectric spectroscopy. The combined dielectric and equation of state data provide a means of disentangling the relative influence of thermal energy and density on the glass "transition". Thermal energy is the controlling parameter of the segmental dynamics in both atactic and isotactic PP as inferred by the values of the ratio of the apparent activation energies at constant pressure and volume (0.72 and 0.63, respectively). Despite the common origin of the segmental dynamics, the relaxation times of the isotactic polymer exhibit higher pressure sensitivity due to the increasing crystallinity on pressurization.

Introduction

Polypropylene (PP) is one of the most common industrial polymers known for its good mechanical properties, processability, and chemical stability. Furthermore, it is not toxic when damaged and is thus suitable for food packaging. Polypropylene can be synthesized in three different tacticities, atactic (aPP), isotactic (iPP), and syndiotactic (sPP), and this microstructure is critical for the physical properties.[1,2] In its well-known isotactic form, it has been used by the industry for many years, but yet is not known how the pressure conditions during the thermoplastic molding affect the physical properties of the final material. Pressures employed during production are in the range 80−800 MPa, which can be reached at the laboratory, under perfectly controlled conditions. The dynamics that are coupled to the processing conditions are the segmental dynamics (called α-process) and the longer range chain dynamics responsible for the flow.

The segmental relaxation times of aPP were studied earlier at atmospheric pressure with creep,[3] dynamic mechanical,[4,5] light scattering,[6] dielectric,[7,8] NMR,[9,10] quasielastic neutron scattering (QENS),[11] and molecular dynamics (MD) simulations.[12,13] There is a general agreement that the segmental dynamics of aPP display strong temperature dependence according to the Vogel−Fulcher−Tammann (VFT) equation. On the other hand, the segmental dynamics of iPP have only been investigated at the high frequency side with QENS[11] and MD simulations.[13] In addition, there are several thermodynamic studies of the equation of state, that is, pressure−volume−temperature (*PVT*) measurements,[14,15] of aPP and iPP, but there exists only one study on the effect of pressure and this on the dynamics of aPP (by deuteron NMR[16]). The latter study revealed a moderate pressure coefficient for the glass temperature. In addition, there are several studies on the effect of shear flow[17] on the crystallization kinetics of iPP and one study[18] where both shear and pressure were applied. In all cases, significantly accelerated crystallization kinetics were obtained.

Pressure experiments over the past decade[19,20] had a large impact in increasing our understanding of the dramatic slowing-down of the α-relaxation times as the system is approaching its glass temperature T_g. There exist two main theoretical considerations of the phenomenon of "glass transition". According to the "energy landscape" theory,[21,22] the α-process is purely thermally activated in a constant density energy landscape and glass formation is attributed to the inability of crossing the energy barriers. On the other hand, in the context of the free volume theory,[23−25] the retardation of the relaxation times results from the lack of sufficient available "free" volume necessary for the motion. These two pictures should be considered as extreme cases; while in the former, the dominant parameter is temperature, in the latter, density (or volume) dominates. It has been demonstrated several times[26−28] that pressure experiments performed under "isothermal" conditions (i.e., at constant thermal energy) can disentangle the effects of temperature and density on the dynamics. The quantification of the relative contribution of temperature and density on the dynamics of the α-process is made by using the ratio of the activation energies at constant volume, $E_V^* = R(\partial \ln \tau/\partial(1/T))_V$, to the enthalpy of activation, $H^* = R(\partial \ln \tau/\partial(1/T))_P$. Ideally, this ratio takes values near 0, when glass formation is controlled only by the free volume, and 1, when thermal energy is the dominant variable.

Herein we investigate the dynamics of a low molecular weight aPP and of a high molecular weight iPP as a function of temperature and pressure. Our aim is 2-fold. First, to obtain quantitative information on the parameter that influences the most the liquid-to-glass transition for the two tacticities. Second, we explore in detail the effect of pressure on the segmental dynamics. This is of interest here for the following reason: iPP is a semicrystalline polymer and pressure is known to affect the crystal thickness, the equilibrium melting temperature and overall crystallinity. On the other hand, aPP is completely amorphous. Will pressure affect the restricted yet amorphous fraction of the isotactic polymer in the same way as in the atactic form? Dielectric spectroscopy as a function of temperature and pressure coupled with the equation of state provides answers to these questions. Information on the crystal structure, crystallinity and the kinetics of crystallization for the iPP are provided in the Supporting Information.

Experimental Section

Samples. Two samples were used for DS experiments, purchased from Polymer Standards. They correspond to a low molecular weight, amorphous PP (sample code: PSS-pp3.5k, herein called aPP, $T_g^{DS} = 258.0$ K) and a high molecular weight, semicrystalline PP

* To whom correspondence should be addressed. E-mail: gfloudas@cc.uoi.gr.

10.1021/ma8014992 CCC: $40.75
Published on Web 11/11/2008

Table 1. Molecular Characteristics of the PP Samples

sample	M_w (g/mol)	M_n (g/mol)	M_p (g/mol)	M_w/M_n	tacticity
aPP	3350	2625	3900	1.28	50% meso dyads
iPP	108000	32500	82800	3.32	99% meso dyads

(sample code: PSS-ppb105k, herein called iPP, $T_g^{DS} = 265.8$ K, $T_g^{DSC} = 265 \pm 7$ K). The molecular characteristics of the samples are tabulated in Table 1. ^{13}C NMR spectra were recorded from o-$C_6D_4Cl_2$ solutions at 393 K. The aPP has entirely head-to-tail linkages with random stereochemistry. The high molecular weight PP is highly isotactic (*mmmm* content ~99%).[29]

Thermal Properties. The thermal behavior of the high molecular weight semicrystalline iPP was examined with a Mettler Toledo Star differential scanning calorimeter (DSC). Approximately 10 mg of the polymer was sealed in an aluminum pan and loaded into the instrument at room temperature. The sample was first cooled at a rate of 10 K/min from ambient temperature to 123 K and then heated to 503 K with the same rate. Two successive cooling and heating runs were performed; the second heating and second cooling thermographs were employed in the analysis of apparent melting points and degree of crystallinity. The results can be found in the Supporting Information (Figure S1). Here we briefly mention that the degree of crystallinity was 45%, estimated as $X_c = \Delta H/\Delta H_\infty$, where ΔH_∞ (=207 J/g) refers to the heat of fusion of a completely crystalline iPP.[2]

Wide-Angle X-ray Scattering (WAXS). WAXS measurements were performed at the Max-Planck Institute in Mainz by using the X-ray beam with pinhole collimation and a two-dimensional detector (Siemens A102647) with 1024 × 1024 pixels. A double graphite monochromator for the Cu Kα radiation (λ=0.154 nm) was used. Measurements of 1 h long were made on heating at 303, 373, and 413 K and on subsequent cooling at 373 and 303 K for iPP, whereas the single measurement at 303 K confirmed the absence of crystallization from the aPP sample. A representative WAXS curve from iPP at 303 K (on cooling) is shown in the Supporting Information (Figure S1). Several diffraction peaks with (*hkl*) Miller indexes of (110), (040), (130), ($\bar{1}$31)/(111), correspond to the reflections from the monoclinic unit cell[30] of isotactic polypropylene (unit cell parameters of $a = 0.665$ nm, $b = 2.076$ nm, $c = 0.65$ nm, with $\beta = 98.67°$, $\alpha = \gamma = 90°$).

Polarized Optical Microscopy (POM). The real-time crystallization and melting of the semicrystalline iPP was followed by POM (representative image in Figure S1). A thin film (~30 μm) of the sample was placed between glasses and introduced into a Linkam THMS 600 hotplate under an Axioskop 40 FL optical microscope. Two polarizers with crossed polarization axes were placed in the light path in order to detect birefringence coming from the sample. The growth of spherulites in real time was followed under isothermal conditions at different crystallization temperatures (T_c) in the range 393−428 K by capturing images with a CCD camera. The linear growth rates were thus determined. Subsequently, following slow heating the corresponding apparent melting temperatures (T_m') were determined from the complete loss of birefringence. The analysis of the crystallization kinetics (Figure S3) resulted in an estimate for the equilibrium melting temperature[31] (Figure S2) that is provided in the Supporting Information.

Dielectric Spectroscopy. Dielectric measurements were made under "isobaric" conditions as a function of temperature and under "isothermal" conditions as a function of pressure. All measurements were performed using a Novocontrol BDS system composed of a Solartron Schlumberger FRA 1260 frequency response analyzer and a broadband dielectric converter for the range 10^{-2} to 10^6 Hz. The temperature for the atmospheric pressure measurements was stabilized by a Novocontrol Quatro cryosystem with N_2 flow and a precision of 0.05 K. The "isobaric" measurements were performed at different temperatures in the range 123.15−423.15 K, at atmospheric pressure. The "isothermal" measurements were made for temperatures in the range from 303.15 to 403.15 K and for pressure up to 300 MPa. The measurements under hydrostatic pressure were carried out in a Novocontrol pressure cell. The pressure setup consists of a temperature controlled cell, hydraulic closing press with air pump, and air pump for hydrostatic test pressure. The sample cell is isolated with a Teflon ring from the surrounding silicone oil that is the pressure transmitting liquid. The "isothermal" frequency sweeps were made with a temperature stability better than ±0.1 K and a pressure stability better than ±2 MPa.

In every case, the complex dielectric permittivity $\varepsilon^* = \varepsilon' - i\varepsilon''$, where ε' is the real and ε'' is the imaginary part, was obtained as a function of frequency ω, temperature T, and pressure P, that is, $\epsilon^*(T,P,\omega)$.[19] The analysis of both T- and P-dependent experiments was made using the empirical equation of Havriliak and Negami (HN)[32]

$$\varepsilon^*(T,P,\omega) = \varepsilon_\infty(T,P) + \frac{\Delta\varepsilon(T,P)}{[1+(i\omega\tau_{HN}(T,P))^m]^n} + \frac{\sigma_0(T,P)}{i\varepsilon_f\omega} \quad (1)$$

where $\varepsilon_\infty(T,P)$ is the high frequency permittivity, $\tau_{HN}(T,P)$ is the characteristic relaxation time in this equation, $\Delta\varepsilon(T,P) = \varepsilon_o(T,P) - \varepsilon_\infty(T,P)$ is the relaxation strength, m, n (with limits $0 < m$, $mn \leq 1$) describe, respectively, the symmetrical and asymmetrical broadening of the distribution of relaxation times, σ_o is the dc-conductivity and ε_f is the permittivity of free space. From τ_{HN}, the relaxation time at maximum loss, τ_{max}, is obtained analytically following

$$\tau_{max} = \tau_{HN}\left[\frac{\sin\left(\frac{\pi m}{2+2n}\right)}{\sin\left(\frac{\pi mn}{2+2n}\right)}\right]^{-1/m} \quad (2)$$

At high temperatures, the derivative of ε' (d ε'/d ln $\omega \sim -(2/\pi)\varepsilon''$) has been used in order to avoid the conductivity contribution. This is especially necessary for the iPP sample (Figure 5). Measurements with high averaging (20 point averaging) were necessary to increase the signal-to-noise ratio for the semicrystalline iPP below its crystallization temperatures. For the "isothermal" measurements made within the pressure cell, small vertical shifts to the dielectric loss data at 0.1 MPa were applied to bring them in coincide with the corresponding "isobaric" data.

Results and Discussion

The thermal (DSC) and structural (WAXS) investigations have shown that PSS-pp3.5 k is atactic (aPP) and hence completely amorphous whereas the PSS-ppb105k is isotactic (iPP) with an equilibrium melting temperature in the range from 449 to 461 K (depending on the evaluation method; Supporting Information) and a degree of crystallinity of about 45%. We turn now to the segmental dynamics by describing first the aPP.

Figure 1 gives representative dielectric loss spectra for the segmental relaxation of aPP under "isobaric" and "isothermal" conditions, respectively, at $P = 0.1$ MPa and at $T = 298$ K. The upturn in the low-frequency side for the "isothermal" data does not originate from the ionic conductivity but is an experimental artifact. The dielectric loss curves were fitted to the HN equation and at each temperature and pressure four parameters were extracted ($T\Delta\varepsilon$, m, n, τ) associated, respectively, with the dielectric strength, the shape of the process and the characteristic relaxation time. The product $T\Delta\epsilon \sim 40$ K, where $\Delta\epsilon$ is the dielectric strength for the segmental process, was nearly independent of temperature for the "isobaric" experiments whereas an increasing strength was found in the "isothermal" experiments associated with the increasing dipolar density upon pressurization. The shape parameters, with values $m = 0.60 \pm 0.03$ and $n = 0.48 \pm 0.05$, were T-independent (time−temperature superposition holds to a good approximation) with a corresponding Kohlrausch−Williams−Watts (KWW) exponent of $\beta \sim 0.36 \pm 0.05$. Different stretching exponents have been reported for the segmental relaxation in aPP: $\beta \sim$

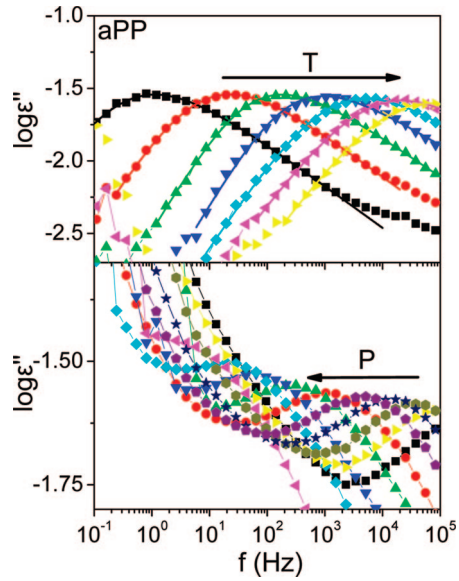

Figure 1. Dielectric loss of aPP as a function of frequency under "isobaric" (top, $P = 0.1$ MPa) and "isothermal" (bottom, $T = 298$ K) conditions. Temperature and pressure increase in the direction of the arrows: $T = 258$ (squares), 263 (circles), 268 (up triangles), 273 (down triangles), 278 (rhombus), 283 (left triangles), and 288 K (right triangles); $P = 0.1$ (squares), 20 (right triangles), 40 (hexagons), 60 (stars), 80 (pentagons), 100 (circles), 120 (up triangles), 140 (down triangles), 160 (rhombi), and 180 MPa (left triangles), respectively. Solid lines to the "isobaric" data are the result of the fit to the HN function.

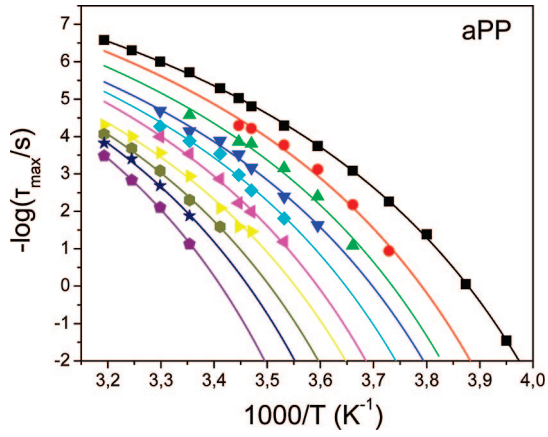

Figure 2. Segmental relaxation times of aPP as a function of temperature at different pressures: 0.1 (squares), 20 (circles), 40 (up triangles), 60 (down triangles), 80 (diamonds), 100 (left triangles), 120 (right triangles), 140 (hexagons), 160 (stars), and 180 MPa (pentagons). The data have been fitted with the VFT equation.

0.56 in the ^{13}C NMR study,[9] $\beta \sim 0.35-0.55$ with a T-dependence in QENS,[11] and $\beta \sim 0.36-0.39$ in the atomistic MD simulations.[12]

The corresponding relaxation times display a strong T-dependence (and P-dependence) characteristic of the segmental (α-) process, which is depicted in Figure 2. The experimental points clearly follow a non-Arrhenius T-dependence that can best be described by the Vogel−Fulcher−Tammann (VFT) equation

$$\tau_{max} = \tau_0 \exp \frac{D_T T_0}{T - T_0} \tag{3}$$

where T_0 (=215 ± 1 K), the ideal glass temperature, τ_0 (=2.5 ± 0.5 × 10^{-12} s), the relaxation time in the very high temperature limit, and D_T (=5.2 ± 0.4), a dimensionless parameter. These relaxation times for the aPP can be compared with the corresponding times from the atomistic MD simulations for a homopolymer of comparable molecular weight.[12] Both sets of data can be fitted with the same VFT curve using $D_T = 5.8$ (see Figure S5a, Supporting Information). Different VFT parameters have been reported based on shifted relaxation times from light scattering,[6] creep,[3] dynamic mechanical,[4,5] dielectric,[7] and NMR[9] measurements ($D_T = 3.93 \pm 0.03$, $T_0 = 234.8 \pm 0.3$), whereas a recent dielectric spectroscopy investigation[8] of aPP (molecular weight of 12000 g/mol) resulted in $D_T = 3.5 \pm 0.4$ and $T_0 = 225 \pm 2$ K. The reason for these discrepancies is mainly the different molecular weights employed in the different studies.

Table 2. Tait Parameters for the Data Used

sample	α_0 (cm^3/g)	α_1 (cm^3/gK)	α_2 (cm^3/gK^2)	B_0 (MPa)	B_1 (K^{-1})
iPP	0.9800	2.8×10^{-4}	5.00×10^{-7}	1400	5.00×10^{-3}
aPP	1.0040	3.7×10^{-4}	6.60×10^{-7}	731	5.11×10^{-3}

Time−pressure superposition (*tP*s) was found to be valid with similar shape parameters ($m = 0.55$ and $n = 0.48$) as at atmospheric pressure (in this case a vertical shift is necessary to account for the increasing dielectric strength with pressure). The corresponding "isothermal" relaxation times, recorded with increasing pressure, where described by the pressure equivalent of VFT[33] as

$$\tau_{max} = \tau_\alpha \exp \frac{D_P P}{P_0 - P} \tag{4}$$

where τ_α is the segmental relaxation time at atmospheric pressure at a given temperature, D_P (=51) is a dimensionless parameter, and P_0 is the pressure corresponding to the ideal glass.

Knowledge of the exact equation of state is essential in the discussion of the parameter that influences glass formation. For this purpose we have employed literature pressure−volume−temperature data[14] (see Figure S4 in Supporting Information) of atactic and isotactic PP below T_m'. The Tait equation was employed for the temperature range where the DS experiments were made

$$\begin{aligned} V(P,T) &= V(0,T)(1 - 0.0894 \ln(1 + P/B(T))) \\ V(0,T) &= a_0 + a_1 T + a_2 T^2 \\ B(T) &= B_0 \exp(-B_1 T) \end{aligned} \tag{5}$$

where α_0, a_1, and a_2 are coefficients of thermal expansion and B_0 and B_1 are parameters that describe the T-dependence of the compressibility. The resulted parameters for both the atactic and the isotactic samples are given in Table 2. Using the above equation of state, the relaxation times under "isobaric" and "isothermal" conditions can be combined using the density as a variable in a $\tau(T, \rho)$ representation. This representation it turns out to be more informative and is depicted in Figure 3. The relaxation times $\tau(T, \rho)$ can now be fitted with the modified VFT function for density[28] as

$$\tau_{max} = \tau_0 \exp \frac{D_\rho \rho}{\rho_0 - \rho} \tag{6}$$

where D_ρ is a dimensionless parameter, τ_0 is the limit of relaxation times at high densities, and ρ_0 is the "ideal glass" density. For the 0.1 MPa data, these parameters are: $\tau_0 = 6 \times 10^{-12}$ s, $D_\rho = 0.67 \pm 0.03$, and $\rho_0 = 0.8970 \pm 0.0008$ g/cm^3.

The degree to which thermal energy and density govern the relaxation times can be assessed from the ratio of the apparent activation energies at constant volume (E^*_V) and pressure (H^*). In turn, the ratio of activation energies, E^*_V/H^*, can be obtained in several ways,[26−28] but a direct way is through the $\tau(T, \rho)$

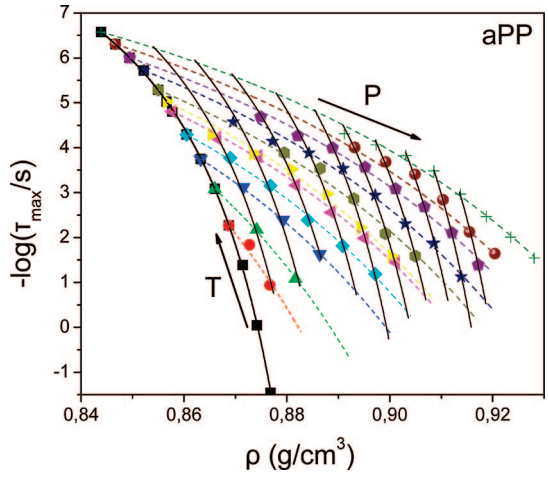

Figure 3. Segmental relaxation times of aPP as a function of density. The lines are fits of the modified VFT equation (eq 8) with density as the independent variable. Isothermal, $D_\rho^T = 2.7$ (dashed lines, $T = 268$ (circles), 273 (up triangles), 278 (down triangles), 283 (rhombi), 288 (left triangles), 290 (right triangles), 293 (hexagons), 298 (stars), 303 (pentagons), 308 (spheres), and 313 K (crosses)); isobaric, $D_\rho^P = 0.67$ (solid lines, $0.1 < P < 200$ MPa in 20 MPa increments; squares, $P = 0.1$ MPa).

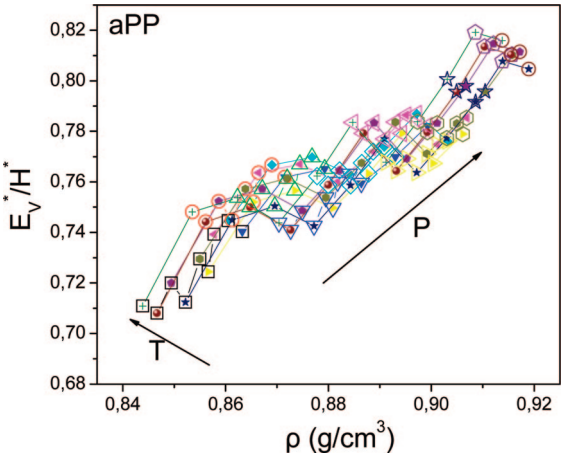

Figure 4. T- and P-dependence of the ratio of activation energies E_V^*/H^* (solid symbols: $T = 278$ (down triangles), 283 (rhombus), 288 (left triangles), 290 (right triangles), 293 (hexagons), 298 (stars), 303 (pentagons), 290 (spheres), and 290 K (cross); open symbols: $P = 0.1$ (squares), 20 (red circles), 40 (up triangles), 60 (down triangles), 80 (rhombi), 100 (left triangles), 120 (right triangles), 140 (hexagons), 160 (stars), 180 (pentagons), and 200 MPa (black circles).

representation from the slopes at the crossing points of the "isothermal" and "isobaric" as

$$\frac{E_V^*}{H^*} = 1 - \frac{(\partial \ln \tau/\partial \rho)_T}{(\partial \ln \tau/\partial \rho)_P} \quad (7)$$

The resulted values are plotted for the aPP in Figure 4 as a function of density. As can be seen, values in the range of 0.71−0.82 are obtained for the different (T,P) conditions investigated. It is worth noticing that the ratio is increasing with pressure. Thus, temperature is the dominant variable of the dynamics at elevated pressures and this can be explained by the increased height of the potential energy barriers thus leading to a more activated behavior. At $P = 0.1$ MPa and at $T = 278$ K, $E^*_V/H^* \sim 0.72 \pm 0.02$. This value suggests that thermal energy and the intramolecular barriers are mostly responsible for the conformational changes associated with the segmental relaxation in aPP. The effect of density on the segmental

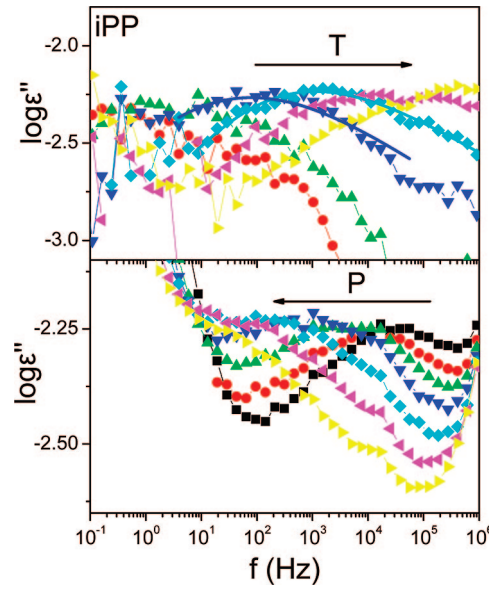

Figure 5. Dielectric loss data of iPP (obtained from the derivative method) as a function of frequency under isobaric (top, $P = 0.1$ MPa) and isothermal (bottom, $T = 303$ K) conditions. Temperature and pressure increase in the direction of the arrows: $T = 263$ (circles), 268 (up triangles), 278 (down triangles), 288 (rhombi), 298 (left triangles), and 308 K (right triangles); $P = 0.1$ (squares), 20 (circles), 40 (up triangles), 60 (down triangles), 80 (rhombi), 100 (left triangles), and 120 MPa (right triangles), respectively. The losses are lower here in comparison to App because of the crystallization of PP. The rise of the intensity at the high-frequency extreme in the bottom graph is an experimental artifact.

relaxation times is not zero, but certainly thermal effects dominate. The barrier heights for such conformational transitions between the dominant (i.e., most populated) rotational isomeric states of aPP (t, g, and $\bar{g}$) have been calculated and are within an order of magnitude within k_BT, for the temperature range investigated.[12] The value of $E^*_V/H^* \sim 0.72$ is in agreement with the pressure-dependent NMR results from ref 16. There a power law scaling $\rho_g(P)^\kappa/T_g(P) =$ constant was found for aPP along the glass transition line with $\kappa = 2$. The exponent κ is another way of quantifying the relative contribution of volume and temperature on the relaxation times and is related directly to the ratio of activation energies.[35]

The same procedure was followed for the high molecular weight crystalline sample (iPP). Figure 5 shows representative dielectric loss spectra under "isobaric" and "isothermal" conditions. Notice the reduced dielectric strength for the α-process as compared to aPP ($T\Delta\epsilon \sim 15$ K) that is due to the smaller fraction of mobile dipoles. In addition, contrary to the aPP case, the dielectric strength does not increase with pressure. As we will see below, this is composite effect resulting from an increasing contribution due to the densified amorphous fraction and a reduced fraction of amorphous segments up on increasing pressure. Time−temperature superposition still holds, however, the spectra are broader than in aPP with $m = 0.36 \pm 0.04$ and $n = 0.55 \pm 0.04$, resulting in a KWW exponent of $\beta \sim 0.27 \pm 0.03$. The earlier published values for iPP are $\beta \sim 0.56$ in ^{13}C NMR, $\beta \sim 0.4-0.55$ with a T-dependence in QENS, and $\beta \sim 0.4-0.46$ in the atomistic MD simulations. A possible origin of this discrepancy could be the higher temperatures employed by the earlier studies and/or the smaller frequency range accessible. The respective relaxation times for the different pressures are compiled in Figure 6. A comparison with the respective times from the atomistic MD simulation is made in Figure S5b, in Supporting Information at two pressures and displays a relatively good agreement. The respective density representation of the relaxation times and the T- and P-

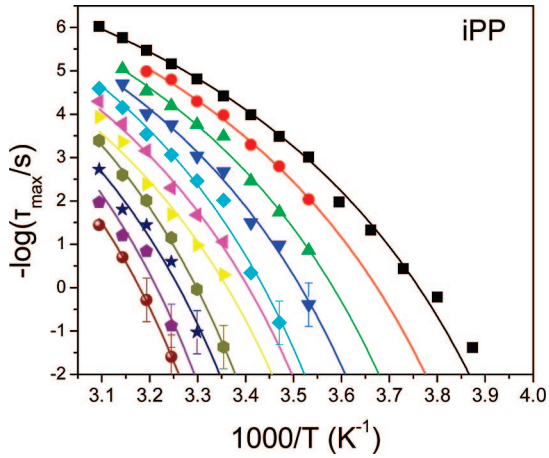

Figure 6. Segmental relaxation times of iPP as a function of temperature at different pressures: 0.1 (squares), 20 (circles), 40 (up triangles), 60 (down triangles), 80 (rhombi), 100 (left triangles), 120 (right triangles), 140 (hexagons), 160 (stars), 180 (pentagons), and 200 MPa (spheres). The data have been fitted with the VFT equation.

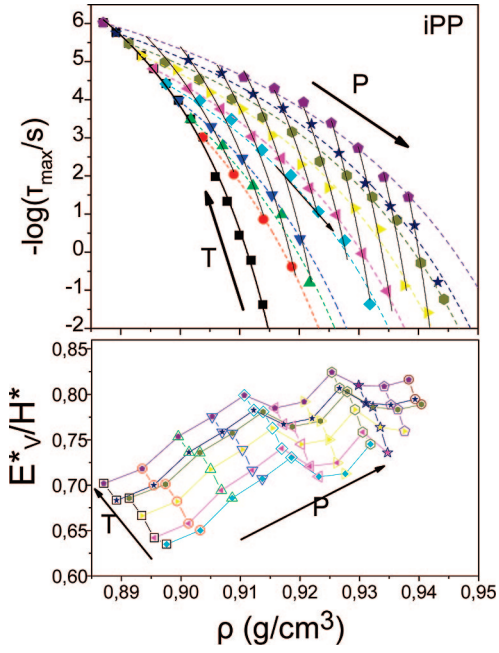

Figure 7. (Top) Segmental relaxation times of iPP as a function of density. The lines are fits of the modified VFT equation (eq 8) with density as the independent variable. Isothermal: $D_\rho^T = 1.3$ (dashed lines, T = 283 (circles), 288 (up triangles), 283 (down triangles), 298 (rhombi), 303 (left triangles), 308 (right triangles), 313 (hexagons), 318 (stars), and 323 K (pentagons)); isobaric: $D_\rho^P = 0.75$ (solid lines, $0.1 < P < 200$ MPa in 20 MPa increments, squares: $P = 0.1$ MPa). (Bottom): Variation of the ratio of activation energies E_V^*/H^* on temperature and pressure (solid symbols: $T = 298$ (rhombi), 303 (left triangles), 308 (right triangles), 313 (hexagons), 318 (stars), and 323 K (pentagons); open symbols: $P = 0.1$ (squares), 20 (red circles), 40 (up triangles), 60 (down triangles), 80 (rhombi), 100 (left triangles), 120 (right triangles), 140 (hexagons), 160 (stars), 180 (pentagons), and 200 MPa (black circles).

dependence of the E_V^*/H^* ratio are also plotted in Figure 7. The ratio now takes values in the range from 0.63 to 0.85. At P = 0.1 MPa and at T = 298 K (i.e., the lowest temperature investigated), $E^*_V/H^* \sim 0.63 \pm 0.05$. As with the aPP, thermal energy is the dominant parameter controlling the segmental dynamics associated with the liquid-to-glass transition.

Thus, in both aPP and iPP, crossing the intramolecular energy barriers exerts the dominant role on the segmental dynamics. Recently, our group suggested[28] that monomer volume and local

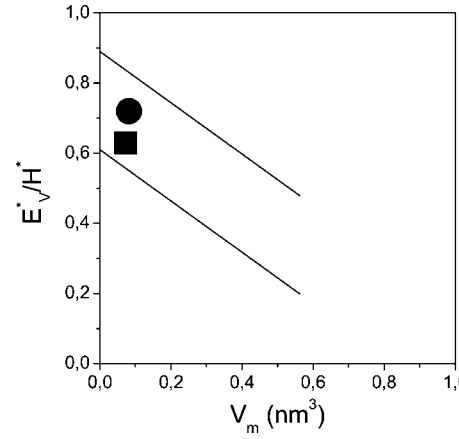

Figure 8. Ratio of activation energies, E_V^*/H^*, as a function of the monomer volume of aPP (circle) and iPP (square). The lines indicate the value boundaries found for most polymers and glass-forming liquids.[28]

packing play a key role in controlling the value of the ratio of activation energies and, thus, the dynamics near T_g. By casting all literature data on the ratio of activation energies as a function of the monomer volume ($V_m = M/\rho N_A$, where M is the monomer molecular weight) an approximate linear relation as $E^*_V/H^* \sim 0.77-0.72V_m$ was proposed.[28] This interrelation is depicted in Figure 8 together with the obtained values for the isotactic and atactic PP. Clearly, the obtained values of aPP and iPP are well within the expected range. Again this suggests that the reason for the high values and relative proximity of the two activation energies is the small monomer volume of PP.

Because of the different molecular weights of the aPP and iPP homopolymers employed herein, we can not test directly the predicted and, to some extent, experimentally observed differences of the segmental times as a function of tacticity. However, there are two quantities where the effect of molecular weight can be scaled-out allowing for a direct comparison. One is the pressure sensitivity of the segmental relaxation times and the second is the pressure sensitivity of the glass temperature itself. With respect to the former, and in analogy to transition state theory (where $\Delta V^{\#}$ is the difference in the molar volumes of activated and nonactivated species) we define an apparent activation volume[19] as

$$\Delta V^{\neq} = 2.303RT\left(\frac{\partial \log \tau_{max}}{\partial P}\right)_T \quad (8)$$

This quantity is calculated from the slope of the $\tau(P)$ dependence at P = 10 MPa, and is depicted for the two PP homopolymers in Figure 9, as a function of temperature difference from the respective T_g. As anticipated from earlier studies,[34,28] it shows a strong temperature dependence on approaching T_g, becoming nearly T-independent at higher temperatures, leveling off to the monomer volume value (~49 cm^3/mol). In the same Figure we include the results from a recent simulation study[13] on iPP, which display a nice agreement with the DS results and with the anticipated monomer value. Notice that the pressure sensitivity of the relaxation times for iPP is stronger than in aPP at all temperatures investigated.

As for the temperature sensitivity of the glass temperature this is depicted in Figure 10, for the aPP and iPP homopolymers (T_g is operationally defined here as the temperature where the relaxation time is τ = 1 s). In a PT diagram the $T_g(P)$ line can be considered as an isochronal line. The filled symbols correspond to isobaric measurements and the open to isothermal

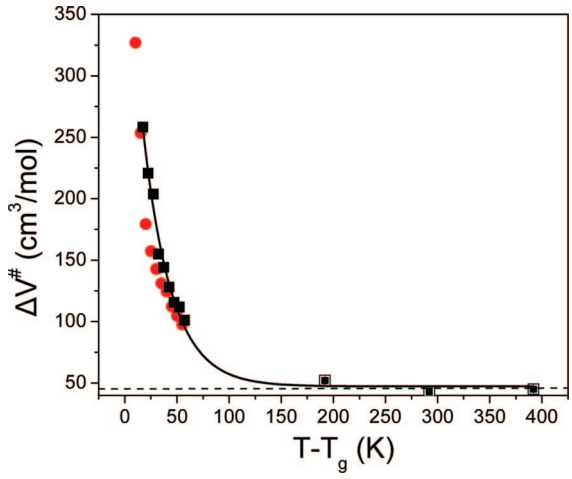

Figure 9. Calculated apparent activation volumes plotted as a function of the temperature difference from the respective T_g for aPP (circles) and iPP (squares). The dashed line corresponds to the monomer volume (~49 cm^3/mol). The open squares are the results from the simulation for an aPP of similar molecular weight.[12]

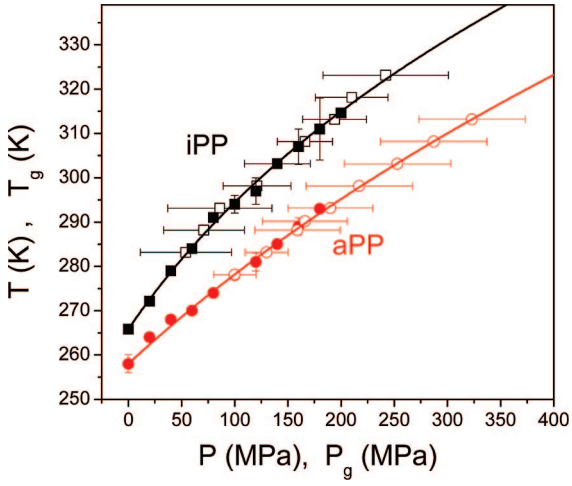

Figure 10. Pressure dependence of the glass temperature, T_g, of the samples investigated: iPP (squares), aPP (circles). The solid symbols correspond to T_g estimated from data in isobaric and the open in isothermal conditions, respectively. The empirical equation (eq 9) has been fitted to the points.

Table 3. Parameters of Eq 9 for the $T_g(P)$ Dependence

sample	$T_g(0)$ (K)	μ (MPa)	ν	$dT_g/dP\|_{P\to 0}$ (K·MPa^{-1})
aPP	258.0	1160	3.5	0.22
iPP	265.8	748	5.0	0.35

ones, respectively. The $T_g(P)$ for the two homopolymers can be described by the following empirical equation

$$T_g(P) = T_g(0)\left(1 + \frac{\nu}{\mu}P\right)^{1/\nu} \quad (9)$$

first proposed by Simon and Glatzel[36] for the melting of solid gases under pressure and subsequently employed by Andersson and Andersson[37] to describe the $T_g(P)$ of glass-forming systems. We mention here parenthetically that an extension of the Simon and Glatzel equation has been proposed for higher pressures.[38] In eq 9, $T_g(0)$ is the glass temperature at atmospheric pressure and ν and μ are fitting parameters. The values of these parameters for aPP and iPP are summarized in Table 3. It can be readily seen from Figure 10 that the initial slope of the curves, that is, the pressure coefficient of T_g ($dT_g/dP|_{P\to 0}$) is significantly higher for the iPP (0.35 K·MPa^{-1}), as compared to the aPP (0.22 K·MPa^{-1}). We mention here that earlier ^{2}H NMR study of the pressure coefficient of T_g yielded a somewhat lower initial slope (0.158 K·MPa^{-1}) for an aPP of 225000 g/mol. The higher pressure coefficient of T_g for the iPP can be understood in terms of the increased crystallinity at elevated pressures. The latter is inferred from the reported[15,18] pressure coefficient of the apparent melting temperature ($dT_m/dP = 0.32$ K/MPa) and the use of the Clausius−Clapeyron equation, $dP/dT_m = \Delta H/T\Delta V$, where T (=443 K) is the transition temperature and ΔV (=0.12 cm^3/g) is the change of volume at atmospheric pressure. The thus calculated heat of fusion under applied pressure ($\Delta H \sim$ 166 J/g) exceeds considerably the heat of fusion for melting of PP crystals at ambient conditions ($\Delta H \sim$ 93 J/g). The "isobaric" PVT measurements performed on the same iPP sample (Supporting Information, Figure S4) on cooling, yield somewhat different values ($dT_c/dP = 0.24$ K/MPa, $\Delta V = 0.09$ cm^3/g, resulting in $\Delta H = 148$ J/g). Nevertheless, both results suggest that pressure increases the crystal thickness by increasing the number of monomer units incorporated within the crystalline lamellar.[39,40] This effectively has as consequences (i) the reduction of the amorphous fraction and (ii) higher conformational constraints on the remaining amorphous segments. The latter is responsible for the higher pressure sensitivity of iPP as compared to the aPP.

Conclusions

The effects of pressure and temperature on the segmental dynamics were investigated in a low molecular weight atactic PP and in a high molecular weight isotactic PP. The ratio of activation energies, E_V^*/H^*, was extracted by coupling the measured relaxation times under "isobaric" and "isothermal" conditions with the known equation of state. From the values of the ratio of activation energies at temperatures near the glass temperature (0.72 ± 0.02 and 0.63 ± 0.05 for the aPP and iPP, respectively) we concluded that the controlling parameter of the segmental dynamics is the thermal energy required to cross the intramolecular energy barriers. Three were the main differences between aPP and iPP. First, the distribution of segmental relaxation times is considerably broader for the iPP ($\beta^{iPP}_{KWW} \sim 0.27$, $\beta^{aPP}_{KWW} \sim 0.36$), and this was anticipated from earlier studies. Second, the apparent activation volume of the iPP is greater than in aPP at all temperatures investigated ($\Delta V^{\#,iPP} > \Delta V^{\#,aPP}$) even after correcting for the difference in glass temperatures, and third, the pressure coefficient of T_g is considerably higher for iPP (0.35 vs 0.22 K/MPa). The latter, with implications in processing, was discussed in terms of the increased crystallinity upon pressurization.

Acknowledgment. This work was cofinanced by the E.U., European Social Fund (75%). and the Greek Ministry of Development. GSRT (25%) in the framework of the program PENED2003 (No 856). We thank Dr. Mihail Mondeshki at MPI-P in Mainz for the ^{1}H and ^{13}C NMR measurements and A. Best for the PVT measurements on the iPP.

Supporting Information Available: Structure characterization (DSC, WAXS, POM), pressure−volume−temperature (*PVT*) parameters, and dynamics comparison. This material is available free of charge via the Internet at http://pubs.acs.org.

References and Notes

(1) Strobl, G. *The Physics of Polymers*; Springer-Verlag: Berlin, 1996; Chapter 4.
(2) (a) Wunderlich, B. *Macromolecular Physics 2. Crystal Nucleation, Growth, Annealing*; Academic Press: New York, 1978. (b) Wunderlich, B. *Thermal Analysis*; Academic Press: New York, 1990, p 418.
(3) Plazek, D. L.; Plazek, D. J. *Macromolecules* **1983**, *16*, 1569.
(4) Pearson, D. S.; Fetters, L. J.; Younghouse, L. B.; Mays, J. W. *Macromolecules* **1988**, *21*, 478.

(5) Santangelo, P. G.; Ngai, K. L.; Roland, C. M. *Macromolecules* **1996**, *29*, 3651.
(6) Fytas, G.; Ngai, K. L. *Macromolecules* **1988**, *21*, 804.
(7) Pakula, T., unpublished.
(8) Kessairi, K.; Napolitano, S.; Capaccioli, S.; Rolla, P.; Wübbenhorst, M. *Macromolecules* **2007**, *40*, 1786.
(9) Lippow, S. M.; Qiu, X.; Ediger, M. D. *J. Chem. Phys.* **2001**, *115*, 4961.
(10) Zemke, K.; Schmidt-Rohr, K.; Spiess, H. W. *Acta Polym.* **1994**, *45*, 148.
(11) Arrighi, V.; Batt-Coutrot, D.; Zhang, C.; Telling, M. T. F.; Triolo, A. *J. Chem. Phys.* **2003**, *119*, 1271.
(12) Antoniadis, S. J.; Samara, C. T.; Theodorou, D. N. *Macromolecules* **1999**, *32*, 8635.
(13) Logotheti, G. E.; Theodorou, D. N. *Macromolecules* **2007**, *40*, 2235.
(14) Zoller, P.; Walsh, D. *Standard pressure-volume-temperature data for polymers*; Technomic Publishing Co. Inc.: Lancaster, Pennsylvania, 1995; pp (a) 47 and (b) 43.
(15) Ito, H.; Tsutsumi, Y.; Minagawa, K.; Takimoto, J.; Koyama, K. *Colloid Polym. Sci.* **1995**, *273*, 811.
(16) Hollander, A. G. S.; Prins, K. O. *J. Non-Cryst. Solids* **2001**, *286*, 1.
(17) (a) Vleeshouwers, S.; Meijer, H. E.H. *Rheol. Acta* **1996**, *35*, 391. (b) Kumaraswamy, G.; Issaian, A. M.; Kornfield, J. A. *Macromolecules* **1999**, *32*, 7537. (c) Tribout, C.; Monasse, B.; Haudin, J. M. *Colloid Polym. Sci.* **1996**, *274*, 197. (d) Janeschitz-Kriegl, H.; Ratajski, E.; Wippel, H. *Colloid Polym. Sci.* **1999**, *277*, 217.
(18) Watanabe, K.; Suzuki, T.; Masubuchi, Y.; Taniguchi, T.; Takimoto, J.; Koyama, K. *Polymer* **2003**, *44*, 5843.
(19) (a) Floudas, G. In *Broadband Dielectric Spectroscopy*; Kremer, F., Schönhals, Eds.; Springer: Berlin, 2002; Chap. 8. (b) Floudas, G. *Prog. Polym. Sci.* **2004**, *29*, 1143.
(20) Roland, C. M.; Paluch, M.; Pakula, T.; Casalini, R. *Philos. Mag.* **2004**, *84*, 1573.
(21) Angell, C. A. *Science* **1995**, *267*, 1924.
(22) Stillinger, F. H. *Science* **1995**, *267*, 1935.
(23) Ferry, J. D. *Viscoelastic Properties of Polymers*, 3rd ed.; Wiley: New York, 1980.
(24) Cohen, M. H.; Grest, G. S. *Phys. Rev. B* **1979**, *20*, 1077.
(25) Bendler, J. T.; Fontanella, J. J.; Shlesinger, M. F. *Phys. Rev. Lett.* **2001**, *87*, 195503.
(26) Naoki, M.; Endou, H.; Matsumoto, K. *J. Phys. Chem.* **1987**, *91*, 4169.
(27) (a) Tölle, A.; Schober, H.; Wuttke, J.; Randl, O. G.; Fujara, F. *Phys. Rev. Lett.* **1998**, *80*, 2374. (b) Tarjus, G.; Kivelson, D.; Mossa, S.; Alba-Simionesco, C. *J. Chem. Phys.* **2004**, *120*, 6135. (c) Casalini, R.; Roland, C. M. *Phys. Rev. E* **2004**, *69*, 062501. (d) Paluch, M.; Casalini, R.; Roland, C. M. *Phys. Rev. B* **2002**, *66*, 092202.
(28) (a) Floudas, G.; Mpoukouvalas, K.; Papadopoulos, P. *J. Chem. Phys.* **2006**, *124*, 074905. (b) Mpoukouvalas, K.; Gomopoulos, N.; Floudas, G.; Herrmann, C.; Hanewald, A.; Best, A. *Polymer* **2006**, *47*, 7241. (c) Mpoukouvalas, K.; Floudas, G. *Macromolecules* **2008**, *41*, 1552.
(29) Zhongde, X.; Mays, J.; Xuexin, C.; Hadjichristidis, N.; Schilling, F. C.; Bair, H. E.; Pearson, D. S.; Fetters, L. J. *Macromolecules* **1985**, *18*, 2560.
(30) Natta, G.; Corradini, P. *Nuovo Cimento, Suppl.* **1960**, *15*, 40.
(31) (a) Marand, H.; Xu, J.; Srinivas, S. *Macromolecules* **1998**, *31*, 8219. (b) Xu, J.; Srinivas, S.; Marand, H. *Macromolecules* **1998**, *31*, 8230.
(32) Havriliak, S.; Negami, S. *Polymer* **1967**, *8*, 161.
(33) Paluch, M.; Patkowski, A.; Fischer, E. W. *Phys. Rev. Lett.* **2000**, *85*, 2140.
(34) (a) Floudas, G.; Reisinger, T. *J. Chem. Phys.* **1999**, *111*, 5201. (b) Floudas, G.; Fytas, G.; Reisinger, T.; Wegner, G. *J. Chem. Phys.* **1999**, *111*, 9129. (c) Floudas, G.; Gravalides, C.; Reisinger, T.; Wegner, G. *J. Chem. Phys.* **1999**, *111*, 9847.
(35) Roland, C. M.; Hensel-Bielowka, S.; Paluch, M.; Casalini, R. *Rep. Prog. Phys.* **2005**, *68*, 1405.
(36) Simon, F. E.; Glatzel, Z. *Z. Anorg. Allg. Chem.* **1929**, *178*, 309.
(37) Andersson, S. P.; Andersson, O. *Macromolecules* **1998**, *31*, 2999.
(38) Drozd-Rzoska, A.; Rzoska, S. J.; Imre, A. R. *J. Non-Cryst. Solids* **2007**, *353*, 3915.
(39) Mierzwa, M.; Floudas, G.; Stepanek, P.; Wegner, G. *Phys. Rev. B* **2000**, *62*, 14012.
(40) Hatakeyama, T.; Kanetsuna, H.; Hashimoto, T. *J. Macromol. Sci., Part B: Phys.* **1973**, *B7*, 411.

MA8014992